Ultrasensitivity of Water Exchange Kinetics to the Size of Metal Ion

Yuno Lee,[†] D. Thirumalai,[‡] and Changbong Hyeon[*,†]

[†]Korea Institute for Advanced Study, Seoul 02455, Korea
[‡]Department of Chemistry, University of Texas, Austin, Texas 78712-1224, United States

S *Supporting Information*

ABSTRACT: Metal ions play a vital role in many biological processes. An important factor in these processes is the dynamics of exchange between ion bound-water molecules and the bulk. Although structural and dynamical properties of labile waters bound to metal ions, such as Na^+ and Ca^{2+}, can be elucidated using molecular dynamics simulations, direct evaluation of rates of exchange of waters rigidly bound to high charge density Mg^{2+}, has been elusive. Here, we report a universal relationship, allowing us to determine the water exchange time on metal ions as a function of valence and hydration radius. The proposed relationship, which covers times spanning 14 orders of magnitude, highlights the ultrasensitivity of water lifetime to the ion size, as exemplified by divalent ions, Ca^{2+} ($\sim$100 ps) and Mg^{2+} ($\sim$1.5 μs). We show that even when structures, characterized by radial distributions are similar, a small difference in hydration radius leads to a qualitatively different (associative or dissociative) mechanism of water exchange. Our work provides a theoretical basis for determination of hydration radius, which is critical for accurately modeling the water dynamics around multivalent ions, and hence in describing all electrostatically driven events such as ribozyme folding and catalysis.

The effect of ions in solution on the surrounding waters is of great interest in chemistry.[1−6] Besides being of fundamental interest, ions play a critical role in the assembly of biopolymers as well as in the conformations of synthetic polymers. Insertion of an ion in solution radially aligns the water molecules and locally perturbs the water hydrogen bond network (see Supporting Information for the effect of ion on H-bond network of water and Figure S1). In contrast to the general notion that water dynamics is faster than the conformational dynamics of biomolecules, the relaxation time of water from biomolecular surfaces can vary widely.[7,8] Remarkably, the water exchange times on metal ion span 18 orders of magnitude in time scales from subnsec for Cs^+ to an extrapolated value of 300 years for Ir^{3+}.[3]

A seemingly minor variation in the size and electric charge leads to dramatic change in the surrounding water.[2] Assessment of gain and loss of energy/entropy in ion−solvent and solvent−solvent interactions is already complicated.[2] To decipher the physical origin of water−ion interaction in detail, quantum mechanical effects, such as polarizations of both ion and water[2,9] and nuclear quantum effects,[10,11] have been explored. From the perspective of classical mechanics, ion is modeled as a sphere with a certain radius and fixed charge. It is, however, difficult to umambiguously choose the effective size of the hydrated ion, so as to mimic the ion−water interaction accurately. The ion size determined from crystallographic structure of salt differs from the value in solution or in gas phase.[2,12] Interestingly, one of the ion parameters (σ^*), corresponding to the van der Waals (vdW) radius parameter for nonbonded Lennard-Jones potential (see Equation S3 for the precise definition) shows significant variations between the force fields (CHARMM27, AMBER03, GROMOS96, GROMOS87). For example, σ^* of Mg^{2+} in CHARMM27 (2.11 Å) is $\sim$50% greater than the one in AMBER03 (1.41 Å) (Table S1). Because of this difference, each force field choose different value of vdW interaction strength ε (Table S1), so as to obtain converged positions of the first (1HS) and second hydration shells (2HS) (r_1^* and r_2^*) (Table S2). However, it still remains to be explored how the dynamical properties of water molecules around ion change with this parametrization. Here, we solve this problem by creating a theoretical basis for predicting the water exchange time for a broad range of ions, thus allowing us to obtain more accurate value of hydration radius (r_1^*) and hence σ^*.

The radial distribution functions of water (water-RDF) around metal ions (Mg^{2+}, Ca^{2+}, and Na^+) show two distinct peaks corresponding to the 1HS and 2HS (Figure 1a,b), which agree well with the values derived from diffraction and EXAFS measurements within $\sim\pm$50% error.[13,14] The stronger inertness of hydration layer around Mg^{2+} is captured by the pronounced water oxygen density and a unique coordination number of water in the 1HS, $CN_1 = 6$, whereas broad distributions of $CN_1 (= 3−10)$ are obtained for Ca^{2+} and Na^+ (Figure S2b).

Evaluations of thermodynamic and kinetic properties of hydrated monovalent ions[15] and relatively large divalent ions using MD simulations are straightforward (SI Methods) because the water exchange time $\sim(10−100)$ ps is in an easily accessible regime using direct MD simulations: $\tau = 21−38.5$ ps for Na^+; $\tau = 117−753$ ps for Ca^{2+} (Figure S4 and Table S3). In contrast, despite its particular relevance to understanding of the folding and function of nucleic acids,[16−20] it is impractical to directly simulate with statistical rigor the spontaneous water exchange on Mg^{2+} that retains more rigid hydration layer.

To estimate time scales of slow transitions, indirect approaches using free energy calculation are employed.[5,21] The potentials of mean forces, PMFs, of water bound to Mg^{2+}, obtained from the umbrella sampling method, indicate that the
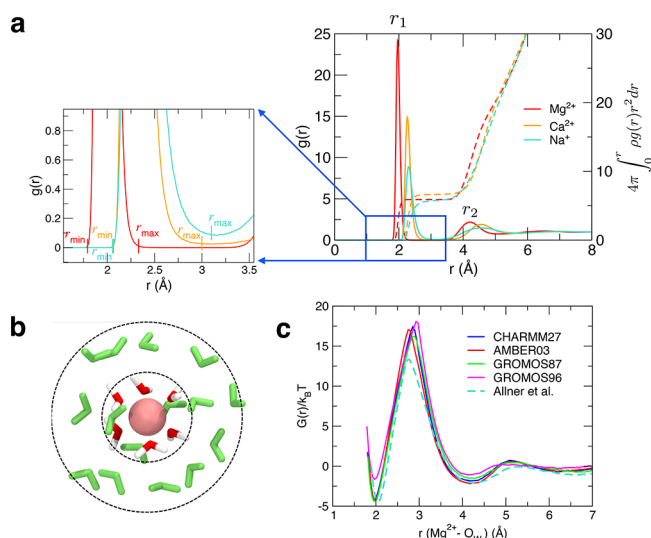
Figure 1. Water structure around metal ions. (a) RDFs of water oxygen around three metal ions (Mg^{2+}, Ca^{2+}, and Na^+) from 100 ns simulations using CHARMM27 force field. The inset on the left depicts the positions of r_{max} and r_{min} that specifies the width of 1HS. (b) Snapshot of water structure around Mg^{2+} from simulations. The surfaces of the 1HS and 2HS are marked with the dashed lines with the water in each shell being depicted in different colors. (c) PMFs, $G(r)$, of water oxygen around Mg^{2+} calculated for four different force fields (solid lines) and Allner et al.'s (dashed line) using umbrella sampling. The free energy barriers for the four force fields are in the range of $\Delta G^{\ddagger}/k_B T = 19.7-21.5$, whereas $\Delta G^{\ddagger}/k_B T = 17.7$ for Allner et al.'s parameters.[5]

kinetic barrier is as large as $\Delta G^{\ddagger}/k_B T = 19.7-21.5$ (Figure 1c). In comparison, the stability of bound water relative to the bulk is only $\Delta G/k_B T = -3\sim-1$ (Figure 1c). Noting that the prefactors of water dissociation from Mg^{2+} and Ca^{2+}, which can be calculated by integrating the PMF,[22] are not qualitatively different (i.e., $\tau_o^{H_2O/Mg^{2+}} \approx \tau_o^{H_2O/Ca^{2+}} \approx 0.24-0.45$ ps), we estimate the water lifetime on Mg^{2+} ion, $\tau_{PMF}^{H_2O/Mg^{2+}} = 130-664$ μs from the Arrhenius-like relationship $\tau = \tau_o e^{\Delta G^{\ddagger}/k_B T}$. However, these values for the force fields tested in this study are 2 orders of magnitude greater than that estimated from NMR measurement.[4]

Alternatively, it is possible to relate the water exchange time with ion valence and the structural features of water-RDF around the ion. Such a relation allows us to predict the water exchange time from structural information on waters, or vice versa. To realize this goal, we carried out kinetic simulations of water exchange dynamics using a pseudomagnesium ion, $Mg^{z+}(\sigma)$, either (i) with a reduced charge ($z < 2$) or (ii) with a bigger vdW radius ($\sigma > \sigma^*$), and extrapolated the results to $z = 2$ and $\sigma = \sigma^*$ where σ^* is the size parameter of Mg^{2+} used (see SI text with Figures S5 and S6 for details). Second, considering the physical basis of water exchange kinetics, we propose the following empirical function in terms of three parameters (z, r_1, r_{max}) as a universal relation onto which all the kinetic data gained from different force fields with varying z and r_1, r_{max} maximally collapse:

$$\log_{10}\tau \sim \alpha \times \frac{z}{r_{max}^3} + \left[\left(\frac{\beta}{r_1}\right)^{12} - \left(\frac{\gamma}{r_1}\right)^6\right] + \delta \times \log_{10}r_1$$
$$+ \varepsilon \tag{1}$$

where α, β, γ, δ, and ε are the 5 parameters to be determined and r_{max} is an upper bound of the width of 1HS (see Figure 1a, inset); more precisely, r_{max} is the smallest value of r in (r_1, r_2) whose $g(r)$ value differs from the minimum value of $g(r)$ by 0.01, i.e., $r_{max} = \min\{r \in (r_1, r_2)||g(r) - \min_{r_1 \leq r \leq r_2}\{g(r)\}| \leq 0.01\}$. The first term z/r_{max}^3 denotes the contribution of ion charge density[19] to the free energy barrier for water unbinding, the second term is associated with Pauli repulsion and van der Waals attraction, and the third and fourth terms are associated with the gain in translational and rotational entropies of water being released from the ion overcoming the activation barrier; the translational entropy is expected to scale as $\sim \log 4\pi r_1^2 \Delta r$, where $\Delta r(=r_{max} - r_{min})$ is the width of 1HS (Figure 1a inset), and the rotational entropy as $\sim k_B T \log \Omega$.

We determine the parameters $\alpha = 19.2$ (Å^3/e), $\beta = 2.50$ (Å), $\gamma = 3.13$ (Å), $\delta = -6.39$, and $\varepsilon = 3.50$, such that all the water exchange times obtained from Na^+, Ca^{2+}, and pseudomagnesium ion (Mg^{z+} with $z = 1.0-1.5$ and Mg^{2+} with varying σ) maximally collapse onto a universal curve. (Note that $\tau_{PMF}^{H_2O/Mg^{2+}}$ estimated from PMF (Figure 1c), x symbols in Figure 2, were not used in the parameter determination. Nevertheless, eq 1 fits the data quantitatively.)
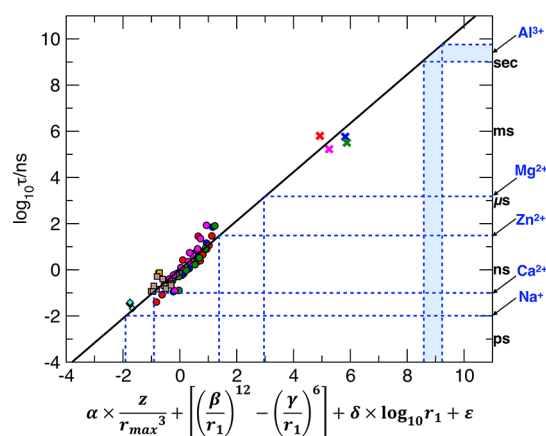

Figure 2. Simulation data of water residence times on pseudomagnesium ion (Mg^{z+}), Na^+ (cyan diamonds), and Ca^{2+} (brown and orange squares) are collapsed on the universal curve (eq 1) with $\alpha = 19.18$ (Å^3/e), $\beta = 2.50$ (Å), $\gamma = 3.13$ (Å), $\delta = -6.39$, $\varepsilon = 3.5$, where the parameters were determined by excluding the results from the PMF analysis for Mg^{2+} (the data points represented with crosses). The correlation coefficient of the data on the curve is ≈0.91. The experimentally determined water lifetimes around Na^+(9.9 ps),[13] Ca^{2+}(<100 ps),[13] Zn^{2+}(32 ns),[24] Mg^{2+}(1.5 μs),[4] and Al^{3+} (1–6 s)[13] are marked with the arrows on the axis to the right.

Equation 1 allows us to predict water dissociation time from an ion using its water-RDF which provides r_1 and r_{max}. The predicted lifetimes of water on Mg^{2+} are 1437 μs (CHARMM27), 164 μs (AMBER03), 1649 μs (GROMOS87), 363 μs (GROMOS96). They are at least comparable with the estimates from PMF calculation, but overestimate the NMR value ($\tau_{exp} = 1.49$ μs)[1,4] by 2 orders of magnitude. The same issue of water lifetime overestimation on Mg^{2+} was discussed by Allnér et al.[5] To resolve this issue, they proposed a new hydration radius $r_1 = 2.04$ Å for Mg^{2+}. To obtain a desired value of τ from eq 1 and Figure 2, it is required that $r_1 \approx 2.04$ Å and $r_{max} \approx 2.37$ Å, regardless of the force field being used. The size parameters for Mg^{2+} of the above four force fields ($\sigma^* = 1.41-$

2.11 Å) (Table S1) yield $r_1 = 1.98-1.99$ Å with $r_{max} \approx 2.31-2.33$ Å, which are only $\sim$2.5% smaller than those required. However, according to eq 1 and Figure 2, this underestimation of r_1 by $\sim$2.5% results in $\sim$400-fold overestimation of τ.

In fact, it is possible to empirically relate r_1^* with σ^* while keeping other parameters being fixed (see SI text). With this mapping, the desired size parameter σ^* of Mg^{2+} is σ^*/Å = 2.42 (CHARMM27), 1.64 (AMBER03), 2.05 (GROMOS87), 2.10 (CGROMOS96), all of which correspond to $\sim$15% increase in vdW radius (diameter $\sim 2^{1/6}\sigma^*$) from those in the original force fields. It is noteworthy that when the parameters by Allnér et al.,[5] which gives rise to $r_1 \approx 2.04$ Å, is used with TIP3P water to calculate PMF, the kinetic barrier for water dissociation is lowered by $\sim$4.1 $k_B T$, whereas the stability of water on Mg^{2+} is barely changed[5] (Figure 1c).

Figure 3, which replots the water lifetimes in Figure 2 as a function of r_1, makes it clear that the water exchange times are
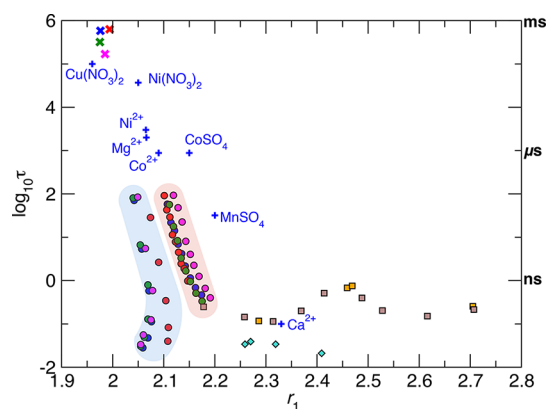
Figure 3. Mean lifetimes of water around various ions as a function of r_1. $Mg^{2+}(\sigma^*)$ with varying z (circles on blue shade), $Mg^{2+}(\sigma)$ with varying $\sigma(>\sigma^*_{Mg^{2+}})$ (circles on pale red shade), Ca^{2+} (orange squares from 4 force fields), $Ca^{2+}(\sigma)$ with varying σ (brown squares, based on CHARMM27), Na^+ (cyan diamonds from 4 force fields), and experimentally determined water lifetimes[13] on various divalent metal ions (blue crosses). Note that τ becomes highly sensitive to r_1 for $r_1 \lesssim 2.2$ Å.

highly sensitive to the hydration radii when $r_1 < 2.2$ Å. The ultrasensitivity of τ on r_1 is also directly confirmed by the collection of data measured for divalent transition metal ions,[13] which cover the time scale over 6 orders (0.1 ns −0.1 ms) in the range of $1.95 < r_1 < 2.33$ Å and are nicely aligned with our simulation data.

As long as d-orbital mediated covalent bonding is not associated with water coordination as in transition metals,[23] our universal curve in Figure 2 can be used to assess the quality of proposed force field for other ions, such as Zn^{2+} and Al^{3+} (Table 1). The water lifetime on Zn^{2+} is $\sim$32 ns,[24] and the water-RDF around Zn^{2+} obtained from CHARMM27 yields the closest value to it (Table 1). For Al^{3+} whose water exchange time is measured $\sim$(1−6) s,[13] eq 1 and Figure 2 indicate that the RDF proposed in ref 25, which conducted *ab initio* MD simulation, gives the most reasonable value of water dissociation time among the four[25−28] in Table 1.

Water exchange dynamics on the labile ions occur within the simulation time scale, allowing us to monitor the process in detail and to categorize it into two distinct mechanisms: associative and dissociative mechanisms.[29] The simulations of water on Ca^{2+} under CHARMM27 force field reveal that $\sim$88%

Table 1. Estimates of Water Exchange Time for Zn^{2+} and Al^{3+} Using eq 1[a]

|	system	r_1 (Å)	r_{max} (Å)	$\log_{10} \tau_{est}/ns$
Zn^{2+}	Zn^{2+} (CHARMM27)	2.10	2.40	1.57
	Zn^{2+} (AMBER03)	1.93	2.36	9.08
	Zn^{2+} (GROMOS96)	2.05	2.39	2.61
	Zn^{2+} (GROMOS87)	2.03	2.35	3.50
Al^{3+}	Bylaska et al.[25]	1.93	2.25	9.80
	Martinez et al.[26]	1.91	2.22	11.90
	Hofer et al.[27]	1.90	2.16	13.32
	Faro et al.[28]	1.86	2.10	19.19

[a](i) For Zn^{2+}, CHARMM27 gives the closest value to the measurement[24] ($\log_{10} \tau/ns = 1.5$). (ii) As the parameters for Al^{3+} are not available in the four biomolecular force fields. Among the water exchange times estimated using four water-RDFs around Al^{3+} available in the literature, Bylaska et al.'s water-RDF yields the closet value to the measurement ($\log_{10} \tau/ns = 9.0-9.8$).[13]

of water exchange events occur via associative mechanism, that is, the association of a bulk water increases the water coordination number on Ca^{2+} from its $CN_1 = 7$ to 8 and return back to 7 after an average lifetime of 2.40 ps (Table S4). However, in AMBER03 and GROMOS force fields, the water exchange occurs mainly via dissociative mechanism, in which CN_1 decreases prior to exchange. Thus, the dominant mechanism of water exchange varies with the force field. In fact, the water exchange mechanism can be determined experimentally by measuring the pressure-dependent variation of rate constant.[30] Although water-RDFs from the four force fields are practically identical (Figures S2a, S3), which gives an initial impression that any force field can be used reliably, a difference in the packing of waters around ion, which arises from the slight difference in the vdW radius, alters water coordination number[31] or activation volume,[30] which in turn alters the water exchange mechanism. The dynamical feature associated water coordination number[31] can also be used to improve the choice of force field and adjustment of size parameter.

Quantum effects that arise from low mass nuclei[32] and electron polarization of ion and water, neglected in this study, certainly contribute to the water exchange dynamics. When explcitly incorporated to classical MD simulations they can improve the water exchange time to an experimentally measured value.[33] Mg^{2+} ion, indeed, has a strong nuclear quantum effects correlated with the longer water residence time.[10,11] Overall, water-RDFs for Ca^{2+} from DFT calculations[34] yield water residence times (114−250 ps) in better agreement with the measured value (<100 ps) than the broadly scattered results from classical force fields (117−753 ps, Table S3). This means that MD force fields only with classical parameters have to be adjusted in accordance with the quantum mechanical contributions. The present study effectively describes the water exchange time in multivalent nontransition metal ions (Ca^{2+}, Mg^{2+}, Zn^{2+}, Al^{3+}) in terms of three classical parameters (z, r_1, r_{max}) and provides a practical instruction of how to adjust them.

Lastly, we compare the hydration layer around Mg^{2+} with that around Ca^{2+} (Figure 4). Mg^{2+} has a strong hexa-coordination of waters on the 1HS. In addition to the strong water−ion interaction energy, the water density in the 1HS is 5 times greater than the bulk ($\rho_w^{first} \approx 5 \times \rho_w^{bulk}$, $\rho_w^{bulk} = 33$ nm$^{-3} \approx 55$ M) (Figure S7b), and the dissociation occurs in $\tau^{(1)} \gtrsim 1$ μs.
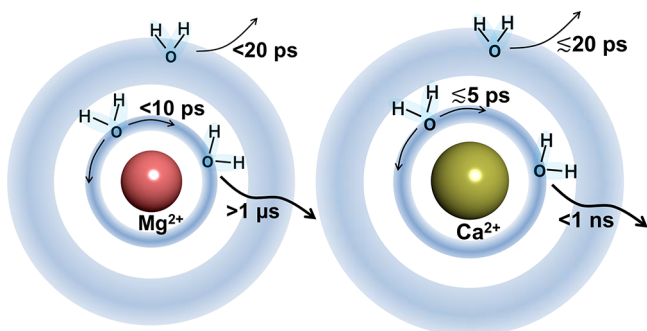
Figure 4. Schematics of water structure around Mg^{2+} and Ca^{2+} recapitulating the simulation results from this study. Specified are the time scales associated with dissociation and orientational relaxation in the 1HS and dissociation from the 2HS.

By contrast, the water density in the 2HS is comparable to the bulk (Figure S7b); and the dissociation time is $\tau^{(2)} < 20$ (ps). Regardless of the ion type (Mg^{2+}, Ca^{2+}, and Na^+) and force field (Table S3), $\tau^{(2)}$ is not significantly different from the bulk water H-bond lifetime (~ 3 ps) (SI text, Figure S7c). The orientational relaxation of water in the 1HS occurs in $\tau_{OR} < 10$ ps (Figure S7c). Although tightly confined to the ~ 0.2 Å layer, the waters in the 1HS are orientally mobile. The ratio of the two time scales $\tau^{(1)}/\tau_{OR}$ for Mg^{2+} is $\sim 10^5$ much greater than $\sim 10^2$ for Ca^{2+}. In the time shorter than the water exchange time, Mg^{2+} can be viewed as a charged sphere of a 3 Å radius, tightly coated with six rotationally mobile water molecules.

The water lifetime on Mg^{2+} ($\sim O(1) \mu s$) is still shorter than the folding time of nucleic acids.[35] Thus, for $\tau \gg O(1) \mu s$, the hydration layer of Mg^{2+} is malleable and the bound waters are free to exchange with the bulk. In crystal structures of RNA, Mg^{2+} ions are directly coordinated to phosphate oxygens, suggesting that a partial desolvation of hexaaqua-magnesium ion occurs during the binding process.[16,36,37] Thus, our work could be used to obtain quantitative insights into ion dynamics during ribozyme folding.

ASSOCIATED CONTENT

S Supporting Information

The Supporting Information is available free of charge on the ACS Publications website at DOI: 10.1021/jacs.7b04198.

Experimental details (PDF)

AUTHOR INFORMATION

Corresponding Author

*hyeoncb@kias.re.kr

ORCID

D. Thirumalai: 0000-0003-1801-5924

Changbong Hyeon: 0000-0002-4844-7237

Notes

The authors declare no competing financial interest.

ACKNOWLEDGMENTS

REFERENCES

(1) Neely, J.; Connick, R. *J. Am. Chem. Soc.* **1970**, *92*, 3476−3678.

(2) Hünenberger, P.; Reif, M. *Single-ion solvation: experimental and theoretical approaches to elusive thermodynamic quantities*; RSC Publishing: Cambridge U. K., 2011.

(3) Cusanelli, A.; Frey, U.; Richens, D. T.; Merbach, A. E. *J. Am. Chem. Soc.* **1996**, *118*, 5265−5271.

(4) Bleuzen, A.; Pittet, P.-A.; Helm, L.; Merbach, A. E. *Magn. Reson. Chem.* **1997**, *35*, 765−773.

(5) Allnér, O.; Nilsson, L.; Villa, A. *J. Chem. Theory Comput.* **2012**, *8* (4), 1493−1502.

(6) Mamatkulov, S.; Fyta, M.; Netz, R. R. *J. Chem. Phys.* **2013**, *138*, 024505.

(7) Lee, Y.; Kim, S.; Choi, S.; Hyeon, C. *Biophys. J.* **2016**, *111*, 1180−1191.

(8) Ostmeyer, J.; Chakrapani, S.; Pan, A. C.; Perozo, E.; Roux, B. *Nature* **2013**, *501*, 121−124.

(9) Halgren, T. A.; Damm, W. *Curr. Opin. Struct. Biol.* **2001**, *11*, 236−242.

(10) Habershon, S. *Phys. Chem. Chem. Phys.* **2014**, *16*, 9154−9160.

(11) Wilkins, D. M.; Manolopoulos, D. E.; Dang, L. X. *J. Chem. Phys.* **2015**, *142*, 064509.

(12) Nightingale, E. R., Jr *J. Phys. Chem.* **1959**, *63*, 1381−1387.

(13) Ohtaki, H.; Radnai, T. *Chem. Rev.* **1993**, *93*, 1157−1204.

(14) Caminiti, R.; Licheri, G.; Piccaluga, G.; Pinna, G. *J. Appl. Crystallogr.* **1979**, *12*, 34−38.

(15) Joung, I. S.; Cheatham, T. E. *J. Phys. Chem. B* **2008**, *112*, 9020−9041.

(16) Misra, V. K.; Draper, D. E. *Proc. Natl. Acad. Sci. U. S. A.* **2001**, *98*, 12456−12461.

(17) Moghaddam, S.; Caliskan, G.; Chauhan, S.; Hyeon, C.; Briber, R. M.; Thirumalai, D.; Woodson, S. A. *J. Mol. Biol.* **2009**, *393*, 753−764.

(18) Koculi, E.; Thirumalai, D.; Woodson, S. A. *J. Mol. Biol.* **2006**, *359*, 446−454.

(19) Koculi, E.; Hyeon, C.; Thirumalai, D.; Woodson, S. A. *J. Am. Chem. Soc.* **2007**, *129*, 2676−2682.

(20) Denesyuk, N. A.; Thirumalai, D. *Nat. Chem.* **2015**, *7*, 793−801.

(21) Whitford, P. C.; Onuchic, J. N.; Sanbonmatsu, K. Y. *J. Am. Chem. Soc.* **2010**, *132*, 13170−13171.

(22) Rey, R.; Hynes, J. T. *J. Phys. Chem.* **1996**, *100*, 5611−5615.

(23) Helm, L.; Merbach, A. E. *Coord. Chem. Rev.* **1999**, *187*, 151−181.

(24) Burgess, J. *Metal ions in solution*; Ellis Horwood Ltd: Chichester, NY, 1978.

(25) Bylaska, E. J.; Valiev, M.; Rustad, J. R.; Weare, J. H. *J. Chem. Phys.* **2007**, *126*, 104505.

(26) Martínez, J. M.; Pappalardo, R. R.; Sánchez Marcos, E. *J. Am. Chem. Soc.* **1999**, *121*, 3175−3184.

(27) Hofer, T. S.; Randolf, B. R.; Rode, B. M. *Chem. Phys. Lett.* **2006**, *422*, 492−495.

(28) Faro, T. M. C.; Thim, G. P.; Skaf, M. S. *J. Chem. Phys.* **2010**, *132*, 114509.

(29) Helm, L.; Merbach, A. E. *Chem. Rev.* **2005**, *105*, 1923−1959.

(30) Rustad, J. R.; Stack, A. G. *J. Am. Chem. Soc.* **2006**, *128*, 14778−14779.

(31) Roy, S.; Baer, M. D.; Mundy, C. J.; Schenter, G. K. *J. Phys. Chem. C* **2016**, *120*, 7597−7605.

(32) Ceriotti, M.; Fang, W.; Kusalik, P. G.; McKenzie, R. H.; Michaelides, A.; Morales, M. A.; Markland, T. E. *Chem. Rev.* **2016**, *116*, 7529−7550.

(33) Dang, L. X. *J. Phys. Chem. C* **2014**, *118*, 29028−29033.

(34) Baer, M. D.; Mundy, C. J. *J. Phys. Chem. B* **2016**, *120*, 1885−1893.

(35) Hyeon, C.; Thirumalai, D. *Biophys. J.* **2012**, *102*, L11−L13.

(36) Kirmizialtin, S.; Elber, R. *J. Phys. Chem. B* **2010**, *114*, 8207−8220.

(37) Cunha, R. A.; Bussi, G. *RNA* **2017**, *23*, 628−638.